Toward the Development of a Three-Dimensional Unconditionally Stable Finite-Difference Time-Domain Method

Fenghua Zheng, *Student Member, IEEE*, Zhizhang Chen, *Senior Member, IEEE*, and Jiazong Zhang

***Abstract*—In this paper, an unconditionally stable three-dimensional (3-D) finite-difference time-method (FDTD) is presented where the time step used is no longer restricted by stability but by accuracy. The principle of the alternating direction implicit (ADI) technique that has been used in formulating an unconditionally stable two-dimensional FDTD is applied. Unlike the conventional ADI algorithms, however, the alternation is performed in respect to mixed coordinates rather than to each respective coordinate direction. Consequently, only two alternations in solution marching are required in the 3-D formulations. Theoretical proof of the unconditional stability is shown and numerical results are presented to demonstrate the effectiveness and efficiency of the method. It is found that the number of iterations with the proposed FDTD can be at least four times less than that with the conventional FDTD at the same level of accuracy.**

***Index Terms*—Alternating direct implicit (ADI) technique, FDTD method, instability, unconditional stable.**

I. Introduction

THE finite-difference time-domain (FDTD) method [1] has been proven to be an effective means that provides accurate predictions of field behaviors for varieties of electromagnetic interaction problems. The FDTD is formulated by directly finite-differencing Maxwell's equations, which leads to a recursive time-marching algorithm where the field solution at the current time step are deduced from the field values at the previous time steps. The basic theory and applications of the FDTD method are well described and can be found in [2].

In general, FDTD is simple and flexible. It can be used to solve various types of electromagnetic problems, such as anisotropic and nonlinear problems. Moreover, since it is a time-domain method, one single run of simulation can provide information over a large bandwidth when the excitation is chosen to be of large bandwidth.

Despite its simplicity and flexibility, the FDTD applications have been limited to solving electrically small structure problems. The main reason is that the FDTD is not yet a computationally efficient technique. For an electrically larger problem, it requires large memory and CPU time to obtain accurate solutions. As a result, computation efficiency becomes the bottleneck for the further applications of the FDTD method.

Theoretical studies on the FDTD show that the intensive memory and CPU time requirements mainly come from the following two modeling constraints ([2] and references therein).

1) The spatial increment step must be small enough in comparison with the smallest wavelength (usually 10–20 steps per smallest wavelength) in order to make the numerical dispersion error negligible.
2) The time step must be small enough so that it satisfies the following Courant stability condition:

$$u_{\max}\Delta t \leq \left[\frac{1}{\Delta x^2}+\frac{1}{\Delta y^2}+\frac{1}{\Delta z^2}\right]^{-1/2} \tag{1}$$

with $u_{\max}$ being the maximum wave phase velocity in the media being modeled. If the time step is not within the bound, the FDTD scheme will become numerically unstable, leading to an unbounded numerical error as a FDTD solution marches.

To circumvent or relax the above constraints, various time-domain techniques have been developed [3]–[8], resulting in the improvement of the computation efficiency. Along the line of relaxing the first constraint, multiresolution time-domain (MRTD) method was proposed by Krumpholz and Katehi [5]. Through the applications of orthonormal wavelet spatial expansions to Maxwell's equations, MRTD scheme can reduce numerical dispersion significantly. The spatial discretization resolution can be made as low as two grid points per wavelength, leading to a large saving in computation memory. Similarly, another technique, the pseudospectral time-domain (PSTD) method, was also developed recently [6]. By using the fast Fourier transform (FFT) to represent spatial derivatives, the PSTD method can also achieve a spatial grid of two points per wavelength while maintaining a high accuracy. Nevertheless, in both cases, the Courant stability conditions remains. For MRTD, the stability condition becomes even more stringent. The time-to-spatial step ratio becomes five times less than that with the conventional FDTD.

To relax or even remove the stability constraint, attempts were made but there have not been many. Early work was reported in 1984 where the alternating-direction-implicit (ADI) technique was first applied to the Yee's grid in order to formulate an implicit FDTD scheme [7]. There, the finite-difference operator for 3D solution of Maxwell's equations was factored into three operators with each operator being performed in respect to the

Manuscript received February 17, 2000.

F. Zheng and J. Zhang are with the Department of Electrical and Computer Engineering, DalTech, Dalhousie University, Halifax, NS B3J 2X4, Canada.

Z. Chen is currently with the Department of Electrical and Electronic Engineering, The Hong Kong University of Science and Technology, Kowloon, Hong Kong, on leave from the Department of Electrical and Computer Engineering, DalTech, Dalhousie University, Halifax, NS B3J 2X4, Canada (e-mail: z.chen@dal.ca).

Publisher Item Identifier S 0018-9480(00)07394-4.

three coordinate directions (namely, x, y, or z). The scheme required three implicit substep computations for each FDTD recursive cycle and it was never found to be completely stable without adding significant dielectric loss. In 1990, a specially designed two-dimensional (2-D) FDTD algorithm, which employs time steps larger than those allowed by methods with explicit time advancement, was presented in [8]. Nevertheless, it is based on a new staggered grid different from Yee's and the grid points and field components are twice of the Yee's on a body surface. Consequently, the method consumes more computer memory and computation resources. Very recently, a new 2-D FDTD algorithm free of the Courant stability conditions was proposed for a 2D-TE wave [9]. The ADI method [11] was again applied [7]. The resulting FDTD formulation was found to be unconditionally stable. Consequently, the second constraint of the FDTD modeling is completely removed. The selection of the FDTD time step is now only dependent on the model accuracy.

In this paper, the ADI principle as applied in [8] is extended to three dimensions, and a *three-dimensional* (3-D) finite-difference time-domain (FDTD) method that is free of the Courant stability condition is consequently developed. Different from the conventional ADI application as appeared in [7] and [9], the ADI here is applied in respect to the sequence of the terms on the right-hand sides (RHSs) of the Maxwell's equations. It then leads to only *two* alternations in the computing direction rather than *three* alternations with the conventional ADI [7]. Moreover, analytical proof of the unconditional stability is provided and numerical experiments that verify the proof are shown. The time step in the proposed FDTD can now be much larger than that with the conventional FDTD.

The paper is organized in the following manners. In Section II, the formulations of the proposed FDTD are described. In Section III, the unconditional stability of the proposed scheme is shown. In Section IV, the numerical results are presented. Finally, in Section V, discussions and conclusions are made in respect to the future directions of the research in the area.

II. Proposed 3-D Unconditionally Stable FDTD Scheme

For simplicity, let's consider an isotropic medium with the medium permittivity ε. The first curl vector equation of Maxwell's equations

$$\nabla \times \mathbf{H} = \varepsilon \frac{\partial \mathbf{E}}{\partial t} \tag{2}$$

can be cast into three scalar partial differential equations in the Cartesian coordinates

$$\frac{\partial E_x}{\partial t} = \frac{1}{\varepsilon}\left(\frac{\partial H_z}{\partial y} - \frac{\partial H_y}{\partial z}\right) \tag{3a}$$

$$\frac{\partial E_y}{\partial t} = \frac{1}{\varepsilon}\left(\frac{\partial H_x}{\partial z} - \frac{\partial H_z}{\partial x}\right) \tag{3b}$$

$$\frac{\partial E_z}{\partial t} = \frac{1}{\varepsilon}\left(\frac{\partial H_y}{\partial x} - \frac{\partial H_x}{\partial y}\right). \tag{3c}$$

In the same way, the second curl vector equation for an isotropic medium with the medium permeability μ

$$\nabla \times \mathbf{E} = -\mu \frac{\partial \mathbf{H}}{\partial t} \tag{4}$$

can be split into three scalar equations

$$\frac{\partial H_x}{\partial t} = \frac{1}{\mu}\left(\frac{\partial E_y}{\partial z} - \frac{\partial E_z}{\partial y}\right) \tag{5a}$$

$$\frac{\partial H_y}{\partial t} = \frac{1}{\mu}\left(\frac{\partial E_z}{\partial x} - \frac{\partial E_x}{\partial z}\right) \tag{5b}$$

$$\frac{\partial H_z}{\partial t} = \frac{1}{\mu}\left(\frac{\partial E_x}{\partial y} - \frac{\partial E_y}{\partial x}\right). \tag{5c}$$

Denote any component of the fields $F_\alpha(t, x, y, z)$ in a discrete space as

$$F_\alpha\big|_{i,j,k}^{n} = F_\alpha(n\Delta t, i\Delta x, j\Delta y, k\Delta z)$$

where $\alpha = x, y,$ or z, n, i, j, k are time and space indexes, Δt is the time step, and $\Delta x, \Delta y, \Delta z$ are the spatial increment steps along the x, y, z directions, respectively.

Consider (3a). By applying the ADI principle that is widely used in solving parabolic equations [11], the computation of (3a) for the FDTD solution marching from the nth time step to the $(n+1)$th time step is broken up into two computational subadvancements: the advancement from the nth time step to the $(n+1/2)$th time step and the advancement from the $(n+1/2)$th time step to the $(n+1)$th time step. More specifically, the two substeps are as follows.

1) For the first half-step (i.e., at the $(n+1/2)$th time step), the *first* partial derivative on the RHS of (3a), $\partial H_z/\partial y$, is replaced with an implicit difference approximation of its unknown pivotal values at $(n+1/2)$th time step; while the *second* partial derivatives on the RHS, $\partial H_y/\partial z$, is replaced with an explicit finite difference approximation in its known values at the previous nth time step. In other words

$$\frac{E_x\big|_{i+\frac{1}{2},j,k}^{n+\frac{1}{2}} - E_x\big|_{i+\frac{1}{2},j,k}^{n}}{\Delta t/2} = \frac{1}{\varepsilon}\left[\frac{H_z\big|_{i+\frac{1}{2},j+\frac{1}{2},k}^{n+\frac{1}{2}} - H_z\big|_{i+\frac{1}{2},j-\frac{1}{2},k}^{n+\frac{1}{2}}}{\Delta y} - \frac{H_y\big|_{i+\frac{1}{2},j,k+\frac{1}{2}}^{n} - H_y\big|_{i+\frac{1}{2},j,k-\frac{1}{2}}^{n}}{\Delta z}\right]. \tag{6}$$

2) For the second half time step (i.e., at $(n+1)$th time step), the second term on the RHS, $\partial H_y/\partial z$, is replaced with an implicit finite-difference approximation of its unknown pivotal values at $(n+1)$th time step; while the first

term, $\partial H_z/\partial y$, is replaced with an explicit finite-difference approximation in its known values at the previous $(n+1/2)$th time step. In other words

$$\frac{E_x|_{i+\frac{1}{2},j,k}^{n+1} - E_x|_{i+\frac{1}{2},j,k}^{n+\frac{1}{2}}}{\Delta t/2} = \frac{1}{\varepsilon}\left[\frac{H_z|_{i+\frac{1}{2},j+\frac{1}{2},k}^{n+\frac{1}{2}} - {}_{n+\frac{1}{2}}H_z|_{i+\frac{1}{2},j-\frac{1}{2},k}^{n+\frac{1}{2}}}{\Delta y} - \frac{H_y|_{i+\frac{1}{2},j,k+\frac{1}{2}}^{n+1} - H_y|_{i+\frac{1}{2},j,k-\frac{1}{2}}^{n+1}}{\Delta z}\right]. \tag{7}$$

Note that the above two substeps represent the alternations in the FDTD recursive computation directions in the sequence of the terms, the *first* and the *second* term. They result in the implicit formulations as the RHSs of the equations contain the field values unknown and to be updated. The technique is then termed "the alternating direction implicit" technique. Attention should also be paid to the fact that no time-step difference (or lagging) between electric and magnetic field components is present in the formulations.

Applying the same procedure to all the other five scalar differential equations as described in (3) and (5), one can obtain the complete set of the implicit unconditionally stable FDTD formulas.

For the advancement from the nth time step, the FDTD equations are listed at the bottom of this page as (8a)–(8f). For the advancement from the $(n+1/2)$th to the $(n+1)$th time step, the FDTD equations are listed at the bottom of the following page as (9a)–(9f). The notations $E_\alpha|_{i,j,k}^n$ and $H_\alpha|_{i,j,k}^h$ with $\alpha = x, y, z$ are the field components with their grid positions being the same as those with the conventional FDTD of the Yee's scheme.

Note that the above ADI procedure is different from the conventional ADI procedure in [7] and [9]. In the conventional ADI procedure, the alternations in the computation directions are made in respect to the three spatial coordinate directions. In the 2-D case, there are two spatial coordinates, e.g., x and y. Therefore, the computations are broken into two substep computations for each temporal cycle (or each time step) (e.g., [9]). The first substep computation is performed in respect to the x direction, while the second computation is performed in respect with the y direction. In the 3-D case, the computations are broken up into three substeps for each cycle since there are three spatial coordinates, x, y, and z (e.g., [7]). In the proposed method, however, the ADI is applied in terms of the sequence of the terms on the RHS of the equations (the *first* and the *second* terms), rather than in terms of the coordinate directions. It then leads to only two alternations in the computation directions in three dimensions. As a result, at each substep, the computations are performed in respect to all the three coordinate directions but with different terms or components. For instance, in (8), one can see that Hz, Hx, and Hy are implicitly computed in respect to the x, y, and z directions, respectively, while in (9) they are explicit for those directions.

Equations (8) and (9) can be further simplified for efficient computations. For instance, consider (8a) where both sides contain the unknown field components. By substituting the expressions for $H_z|_{i+(1/2),j+(1/2),k}^{n+(1/2)}$ and $H_z|_{i+(1/2),j-(1/2),k}^{n+(1/2)}$ represented by (8f) into (8a), one can obtain

$$-\left(\frac{\Delta t^2}{4\mu\varepsilon\Delta y^2}\right)E_x|_{i+\frac{1}{2},j+1,k}^{n+\frac{1}{2}} + \left(1+\frac{\Delta t^2}{2\mu\varepsilon\Delta y^2}\right)E_x|_{i+\frac{1}{2},j,k}^{n+\frac{1}{2}}$$

$$\frac{E_x|_{i+\frac{1}{2},j,k}^{n+\frac{1}{2}} - E_x|_{i+\frac{1}{2},j,k}^{n}}{\Delta t/2} = \frac{1}{\varepsilon}\left[\frac{H_z|_{i+\frac{1}{2},j+\frac{1}{2},k}^{n+\frac{1}{2}} - H_z|_{i+\frac{1}{2},j-\frac{1}{2},k}^{n+\frac{1}{2}}}{\Delta y} - \frac{H_y|_{i+\frac{1}{2},j,k+\frac{1}{2}}^{n} - H_y|_{i+\frac{1}{2},j,k-\frac{1}{2}}^{n}}{\Delta z}\right] \tag{8a}$$

$$\frac{E_y|_{i,j+\frac{1}{2},k}^{n+\frac{1}{2}} - E_x|_{i,j+\frac{1}{2},k}^{n}}{\Delta t/2} = \frac{1}{\varepsilon}\left[\frac{H_x|_{i,j+\frac{1}{2},k+\frac{1}{2}}^{n+\frac{1}{2}} - H_z|_{i,j+\frac{1}{2},k-\frac{1}{2}}^{n+\frac{1}{2}}}{\Delta z} - \frac{H_z|_{i+\frac{1}{2},j+\frac{1}{2},k}^{n} - H_z|_{i-\frac{1}{2},j+\frac{1}{2},k}^{n}}{\Delta x}\right] \tag{8b}$$

$$\frac{E_z|_{i,j,k+\frac{1}{2}}^{n+\frac{1}{2}} - E_z|_{i,j,k+\frac{1}{2}}^{n}}{\Delta t/2} = \frac{1}{\varepsilon}\left[\frac{H_y|_{i+\frac{1}{2},j,k+\frac{1}{2}}^{n+\frac{1}{2}} - H_y|_{i-\frac{1}{2},j,k+\frac{1}{2}}^{n+\frac{1}{2}}}{\Delta x} - \frac{H_z|_{i,j+\frac{1}{2},k+\frac{1}{2}}^{n} - H_x|_{i,j-\frac{1}{2},k+\frac{1}{2}}^{n}}{\Delta y}\right] \tag{8c}$$

$$\frac{H_x|_{i,j+\frac{1}{2},k+\frac{1}{2}}^{n+\frac{1}{2}} - H_x|_{i,j+\frac{1}{2},k+\frac{1}{2}}^{n}}{\Delta t/2} = \frac{1}{\mu}\left[\frac{E_y|_{i,j+\frac{1}{2},k+1}^{n+\frac{1}{2}} - E_y|_{i,j+\frac{1}{2},k}^{n+\frac{1}{2}}}{\Delta z} - \frac{E_z|_{i,j+1,k+\frac{1}{2}}^{n} - E_z|_{i,j,k+\frac{1}{2}}^{n}}{\Delta y}\right] \tag{8d}$$

$$\frac{H_y|_{i+\frac{1}{2},j,k+\frac{1}{2}}^{n+\frac{1}{2}} - H_y|_{i+\frac{1}{2},j,k+\frac{1}{2}}^{n}}{\Delta t/2} = \frac{1}{\mu}\left[\frac{E_z|_{i+1,j,k+\frac{1}{2}}^{n+\frac{1}{2}} - E_z|_{i,j,k+\frac{1}{2}}^{n+\frac{1}{2}}}{\Delta x} - \frac{E_x|_{i+\frac{1}{2},j,k+1}^{n} - E_x|_{i+\frac{1}{2},j,k}^{n}}{\Delta z}\right] \tag{8e}$$

$$\frac{H_z|_{i+\frac{1}{2},j+\frac{1}{2},k}^{n+\frac{1}{2}} - H_z|_{i+\frac{1}{2},j+\frac{1}{2},k}^{n}}{\Delta t/2} = \frac{1}{\mu}\left[\frac{E_x|_{i+\frac{1}{2},j+1,k}^{n+\frac{1}{2}} - E_x|_{i+\frac{1}{2},j,k}^{n+\frac{1}{2}}}{\Delta y} - \frac{E_y|_{i+1,j+\frac{1}{2},k}^{n} - E_y|_{i,j+\frac{1}{2},k}^{n}}{\Delta x}\right]. \tag{8f}$$

$$
\begin{aligned}
&- \left(\frac{\Delta t^2}{4\mu\varepsilon\Delta y^2}\right) E_{x_{i+\frac{1}{2},j-1,k}}^{n+\frac{1}{2}} \\
&= E_x\,|_{i+\frac{1}{2},j,k}^{n} + \frac{\Delta t}{2\varepsilon\Delta y}\left(H_z\,|_{i+\frac{1}{2},j+\frac{1}{2},k}^{n} - H_z\,|_{i+\frac{1}{2},j-\frac{1}{2},k}^{n}\right) \\
&\quad - \frac{\Delta t}{2\varepsilon\Delta z}\left(H_y\,|_{i+\frac{1}{2},j,k+\frac{1}{2}}^{n} - H_y\,|_{i+\frac{1}{2},j,k-\frac{1}{2}}^{n}\right) \\
&\quad - \frac{\Delta t^2}{4\mu\varepsilon\Delta y\Delta x}\left(E_y\,|_{i+1,j+\frac{1}{2},k}^{n} - E_y\,|_{i,j+\frac{1}{2},k}^{n}\right. \\
&\quad \left. - E_y\,|_{i+1,j-\frac{1}{2},k}^{n} + E_y\,|_{i,j-\frac{1}{2},k}^{n}\right). \qquad (10)
\end{aligned}
$$

In it, all the field components on the RHS are of known values at the previous time steps, while the field components on the left-hand side (LHS) are of the same field component, E_x, but at three adjacent grid points.

The same procedures can be applied to (8b)–(9f) and similar equations can be obtained for the other field components. Another easy way is to permute the indexes of the (10). The resulting equations form a linear system of equations that can be solved with available numerical packages. In the following paragraphs, we will describe the approach to the solutions in a matrix form.

In general, (10) and the other similar equations for other field components can be summarized a matrix form

$$\mathbf{M}_1\mathbf{X}^{n+\frac{1}{2}} = \mathbf{P}_1\mathbf{X}^n$$

(for advancement from nth to $(n+1/2)$th time step) (11)

$$\mathbf{M}_2\mathbf{X}^{n+1} = \mathbf{P}_2\mathbf{X}^{n+\frac{1}{2}}$$

(for advancement from $(n+1/2)$th to $(n+1)$th time step). (12)

Here, vector $\mathbf{X}^n$ is a one-column vector containing all the field components at the nth time step. $\mathbf{M}_1, \mathbf{M}_2, \mathbf{P}_1$, and $\mathbf{P}_2$ are the coefficient matrices with their elements related to values of spatial and temporal steps. They are all sparse matrices. $\mathbf{M}_1$ and $\mathbf{M}_2$ are associated with the LHS of (10) while $\mathbf{P}_1$ and $\mathbf{P}_2$ are associated with the RHS of the equations. As can be seen from (10), each row of $\mathbf{M}_1$ and $\mathbf{M}_2$ contains only three nonzero elements at maximum. Maxtrix operations on them can be fast, in particular, the inverse of $\mathbf{M}_1$ and $\mathbf{M}_2$.

Recursive (11) and (12) can be solved either implicitly or explicitly. Since the inverse of the sparse matrix $\mathbf{M}_1$ and $\mathbf{M}_2$ can be found relatively easily, an explicit method is used in our case. That is

$$\mathbf{X}_{n+\frac{1}{2}} = \mathbf{M}_1^{-1}\mathbf{P}_1\mathbf{X}^n \qquad (13)$$

$$\mathbf{X}_{n+1} = \mathbf{M}_2^{-1}\mathbf{P}_2\mathbf{X}^{n+\frac{1}{2}}. \qquad (14).$$

Combination of the above two equations reads

$$\mathbf{X}^{n+1} = \mathbf{M}_2^{-1}\mathbf{P}_2\mathbf{M}_1^{-1}\mathbf{P}_1\mathbf{X}^n \qquad (15)$$

or

$$\mathbf{X}^{n+1} = \mathbf{\Lambda}\mathbf{X}^n$$

with $\mathbf{\Lambda} = \mathbf{M}_2^{-1}\mathbf{P}_2\mathbf{M}_1^{-1}\mathbf{P}_1$.

In an actual simulation, (13) and (14) are computed successively to each other. However, M_1^{-1} or M_2^{-1} may not be needed for calculating all the field values. They may be used only to calculate the field values at the two left-most grid points. For example, consider (10). M_1^{-1} can be used only to calculate, via (13), the left-most values of E_x, say at $j = 0$ and $j = 1$ at the $(n + (1/2))$th time step. The rest of the E_x's can then be calculated by applying (10) with a sequence of ascending j that

$$\frac{E_x\,|_{i+\frac{1}{2},j,k}^{n+1} - E_x\,|_{i+\frac{1}{2},j,k}^{n+\frac{1}{2}}}{\Delta t/2} = \frac{1}{\varepsilon}\left[\frac{H_z\,|_{i+\frac{1}{2},j+\frac{1}{2},k}^{n+\frac{1}{2}} - H_z\,|_{i+\frac{1}{2},j-\frac{1}{2},k}^{n+\frac{1}{2}}}{\Delta y} - \frac{H_y\,|_{i+\frac{1}{2},j,k+\frac{1}{2}}^{n+1} - H_y\,|_{i+\frac{1}{2},j,k-\frac{1}{2}}^{n+1}}{\Delta z}\right] \qquad (9a)$$

$$\frac{E_y\,|_{i,j+\frac{1}{2},k}^{n+1} - E_y\,|_{i,j+\frac{1}{2},k}^{n+\frac{1}{2}}}{\Delta t/2} = \frac{1}{\varepsilon}\left[\frac{H_x\,|_{i,j+\frac{1}{2},k+\frac{1}{2}}^{n+\frac{1}{2}} - H_x\,|_{i,j+\frac{1}{2},k-\frac{1}{2}}^{n+\frac{1}{2}}}{\Delta z} - \frac{H_z\,|_{i+\frac{1}{2},j+\frac{1}{2},k}^{n+1} - H_z\,|_{i-\frac{1}{2},j+\frac{1}{2},k}^{n+1}}{\Delta x}\right] \qquad (9b)$$

$$\frac{E_z\,|_{i,j,k+\frac{1}{2}}^{n+1} - {}_{n+\frac{1}{2}}E_z\,|_{i,j,k+\frac{1}{2}}^{n+\frac{1}{2}}}{\Delta t/2} = \frac{1}{\varepsilon}\left[\frac{H_y\,|_{i+\frac{1}{2},j,k+\frac{1}{2}}^{n+\frac{1}{2}} - H_y\,|_{i-\frac{1}{2},j,k+\frac{1}{2}}^{n+\frac{1}{2}}}{\Delta x} - \frac{H_x\,|_{i,j+\frac{1}{2},k+\frac{1}{2}}^{n+1} - H_x\,|_{i,j-\frac{1}{2},k+\frac{1}{2}}^{n+1}}{\Delta y}\right] \qquad (9c)$$

$$\frac{H_x\,|_{i,j+\frac{1}{2},k+\frac{1}{2}}^{n+1} - H_x\,|_{i,j+\frac{1}{2},k+\frac{1}{2}}^{n+\frac{1}{2}}}{\Delta t/2} = \frac{1}{\mu}\left[\frac{E_y\,|_{i,j+\frac{1}{2},k+1}^{n+\frac{1}{2}} - E_y\,|_{i,j+\frac{1}{2},k}^{n+\frac{1}{2}}}{\Delta z} - \frac{E_z\,|_{i,j+1,k+\frac{1}{2}}^{n+1} - E_z\,|_{i,j,k+\frac{1}{2}}^{n+1}}{\Delta y}\right] \qquad (9d)$$

$$\frac{H_y\,|_{i+\frac{1}{2},j,k+\frac{1}{2}}^{n+1} - H_y\,|_{i+\frac{1}{2},j,k+\frac{1}{2}}^{n+\frac{1}{2}}}{\Delta t/2} = \frac{1}{\mu}\left[\frac{E_z\,|_{i+1,j,k+\frac{1}{2}}^{n+\frac{1}{2}} - E_z\,|_{i,j,k+\frac{1}{2}}^{n+\frac{1}{2}}}{\Delta x} - \frac{E_x\,|_{i+\frac{1}{2},j,k+1}^{n+1} - E_x\,|_{i+\frac{1}{2},j,k}^{n+1}}{\Delta z}\right] \qquad (9e)$$

$$\frac{H_z\,|_{i+\frac{1}{2},j+\frac{1}{2},k}^{n+1} - H_z\,|_{i+\frac{1}{2},j+\frac{1}{2},k}^{n+\frac{1}{2}}}{\Delta t/2} = \frac{1}{\mu}\left[\frac{E_x\,|_{i+\frac{1}{2},j+1,k}^{n+\frac{1}{2}} - E_x\,|_{i+\frac{1}{2},j,k}^{n+\frac{1}{2}}}{\Delta y} - \frac{E_y\,|_{i+1,j+\frac{1}{2},k}^{n+1} - E_y\,|_{i,j+\frac{1}{2},k}^{n+1}}{\Delta x}\right]. \qquad (9f)$$

allows us to find E_x at $j+1$ from E_xs at j and $j-1$. In such a way, for most of the computations, we avoid the application of M_1^{-1} that is not necessarily very sparse. Thus, the computation efficiency can be improved. In addition, after all the electric field components are obtained, magnetic field components can be calculated directly from (8d)–(8f) and (9d)–(9f) with the electic field components already updated.

III. Stability Analysis of the Proposed FDTD Scheme

Generally, for a recursive scheme or system

$$\mathbf{X}^{n+1} = \mathbf{\Lambda} \cdot \mathbf{X}^n \tag{16}$$

its numerical stability can then be determined with the so-called *Fourier* method as described in [10]. In it, instantaneous values of electric and magnetic fields distributed in space across a grid are first *Fourier*-transformed into the waves in the spatial spectral domain to represent a spectrum of spatial sinusoidal modes. Then, by checking the eigenvalues of the $\mathbf{\Lambda}$ with the spectral-domain waves in the system, one can determine the stability conditions of the system. If magnitudes of all the eigenvalues are less than or equal to unity, the scheme is stable. If one of them is larger than one, the scheme is potentially unstable. The *Fourier* method is applied in this paper and the analysis is presented in the following paragraphs.

Assuming the spatial frequencies to be k_x, k_y, and k_z along the x, y, and z directions, the field components in the spatial spectral domain can be writen as

$$E_x\,|^n_{i+\frac{1}{2},j,k} = E_x^n e^{-j(k_x(i+\frac{1}{2})\Delta x + kyj\Delta y + k_z k\Delta z)} \tag{17a}$$

$$E_y\,|^n_{i,j+\frac{1}{2},k} = E_y^n e^{-j(k_x i\Delta x + k_y(j+\frac{1}{2})\Delta y + k_z k\Delta z)} \tag{17b}$$

$$E_z\,|^n_{i,j,k+\frac{1}{2}} = E_z^n e^{-j(k_x i\Delta x + k_y j\Delta y + k_z(k+\frac{1}{2})\Delta z)} \tag{17c}$$

$$H_x\,|^n_{i,j+\frac{1}{2},k+\frac{1}{2}} = H_x^n e^{-j(k_x i\Delta x + k_y(j+\frac{1}{2})\Delta y + k_z(k+\frac{1}{2})\Delta z)} \tag{17d}$$

$$H_y\,|^n_{i+\frac{1}{2},j,k+\frac{1}{2}} = H_y^n e^{-j(k_x(i+\frac{1}{2})\Delta x + k_y j\Delta y + k_z(k+\frac{1}{2})\Delta z)} \tag{17e}$$

$$H_z\,|^n_{i+\frac{1}{2},j+\frac{1}{2},k} = H_z^n e^{-j(k_x(i+\frac{1}{2})\Delta x + k_y(j+\frac{1}{2})\Delta y + k_z k\Delta z)}. \tag{17f}$$

Substitution of these equations into (8) and (9), respectively, can lead to (16) in the spatial spectral domain in terms of $k_x, k_y, k_z, \Delta t, \Delta x, \Delta y$, and Δz.

Denote the field vector in the spatial spectral domain as

$$\mathbf{X}^n = \begin{bmatrix} E_x^n \\ E_y^n \\ E_z^n \\ H_x^n \\ H_y^n \\ H_z^n \end{bmatrix}$$

Then the time-marching relation can be written in a matrix form as

$$\mathbf{X}^{n+\frac{1}{2}} = \mathbf{\Lambda}_1 \cdot \mathbf{X}^n \tag{18}$$

where

$$\mathbf{\Lambda}_1 = \begin{bmatrix} \frac{1}{Q_y} & \frac{W_x \cdot W_y}{\mu\varepsilon Q_y} & 0 & 0 & \frac{jW_z}{\varepsilon Q_y} & \frac{-jW_y}{\varepsilon Q_y} \\ 0 & \frac{1}{Q_z} & \frac{W_z \cdot W_y}{\mu\varepsilon Q_z} & \frac{-jW_z}{\varepsilon Q_z} & 0 & \frac{jW_x}{\varepsilon Q_z} \\ \frac{W_x \cdot W_z}{\mu\varepsilon Q_x} & 0 & \frac{1}{Q_x} & \frac{jW_y}{\varepsilon Q_x} & \frac{-jW_x}{\varepsilon Q_x} & 0 \\ 0 & \frac{-jW_z}{\mu Q_z} & \frac{jW_z}{\mu Q_z} & \frac{1}{Q_z} & \frac{W_x \cdot W_z}{\mu\varepsilon Q_z} & \\ \frac{jW_z}{\mu Q_x} & 0 & \frac{-jW_x}{\mu Q_x} & \frac{W_x \cdot W_y}{\mu\varepsilon Q_x} & \frac{1}{Q_x} & 0 \\ \frac{-jW_y}{\mu Q_y} & \frac{jW_x}{\mu Q_y} & 0 & 0 & \frac{W_z \cdot W_y}{\mu\varepsilon Q_y} & \frac{1}{Q_y} \end{bmatrix}$$

$$W_\alpha = \frac{\Delta t}{\Delta \alpha} \cdot \sin\left(\frac{k_\alpha \Delta \alpha}{2}\right), \qquad \alpha = x, y, z$$

$$Q_\alpha = 1 + \frac{W_\alpha^2}{\mu\varepsilon}, \qquad \alpha = x, y, z$$

and

$$\mathbf{X}^{n+1} = \mathbf{\Lambda}_2 \cdot \mathbf{X}^{n+\frac{1}{2}} \tag{19}$$

where

$$\mathbf{\Lambda}_2 = \begin{bmatrix} \frac{1}{Q_z} & 0 & \frac{W_z \cdot W_x}{\mu\varepsilon Q_z} & 0 & \frac{jW_z}{\varepsilon Q_z} & \frac{-jW_y}{\varepsilon Q_z} \\ \frac{W_x \cdot W_y}{\mu\varepsilon Q_x} & \frac{1}{Q_x} & 0 & \frac{-jW_z}{\varepsilon Q_x} & 0 & \frac{jW_x}{\varepsilon Q_x} \\ 0 & \frac{W_y \cdot W_z}{\mu\varepsilon Q_y} & \frac{1}{Q_y} & \frac{jW_y}{\varepsilon Q_y} & \frac{-jW_x}{\varepsilon Q_y} & 0 \\ 0 & \frac{-jW_z}{\mu Q_y} & \frac{jW_y}{\mu Q_y} & \frac{1}{Q_y} & \frac{W_z \cdot W_y}{\mu\varepsilon Q_y} & 0 \\ \frac{jW_z}{\mu Q_z} & 0 & \frac{-jW_x}{\mu Q_z} & 0 & \frac{1}{Q_z} & \frac{W_z \cdot W_y}{\mu\varepsilon Q_z} \\ \frac{-jW_y}{\mu Q_x} & \frac{jW_x}{\mu Q_x} & 0 & 0 & \frac{W_z \cdot W_x}{\mu\varepsilon Q_x} & \frac{1}{Q_x} \end{bmatrix}$$

Substitution of (18) into (19) reads

$$\mathbf{X}^{n+1} = \mathbf{\Lambda}\mathbf{F}^n = \mathbf{\Lambda}_1\mathbf{\Lambda}_2\mathbf{X}^n. \tag{20}$$

With the use of Maple V5.2, we can obtain (21), shown at the bottom of the next page, where

$$\begin{aligned} W &= W_x W_y W_z \\ A_1 &= \mu^3\varepsilon^3 + \mu^2\varepsilon^2\left(W_x^2W_y^2W_z^2\right) + W_x^2W_y^2W_z^2 \\ A_2 &= \mu^3\varepsilon^3 + \mu^2\varepsilon^2\left(W_y^2W_z^2W_x^2\right) + W_x^2W_y^2W_z^2 \\ A_3 &= \mu^3\varepsilon^3 + \mu^2\varepsilon^2\left(W_z^2W_x^2W_y^2\right) + W_x^2W_y^2W_z^2 \\ B_1 &= \mu\varepsilon\left(W_x^2W_y^2 - W_y^2W_z^2 - W_z^2W_x^2\right) \\ B_2 &= \mu\varepsilon\left(W_y^2W_z^2 - W_z^2W_x^2 - W_x^2W_y^2\right) \\ B_3 &= \mu\varepsilon\left(W_z^2W_x^2 - W_x^2W_y^2 - W_y^2W_z^2\right) \\ D_1 &= W_y\left(W_x^2W_z^2 - \mu^2\varepsilon^2\right) \\ D_2 &= W_z\left(W_y^2W_x^2 - \mu^2\varepsilon^2\right) \\ D_3 &= W_x\left(W_z^2W_y^2 - \mu^2\varepsilon^2\right). \end{aligned}$$

The eigenvalues of $\mathbf{\Lambda}$ can then be found, again with the help of MAPLE, as

$$\begin{aligned} \lambda_1 &= \lambda_2 = 1 \\ \lambda_3 &= \lambda_5 = \frac{\sqrt{R^2 - S^2} + jS}{R} \\ \lambda_4 &= \lambda_6 = \lambda_3^* = \frac{\sqrt{R^2 - S^2} - jS}{R} \end{aligned} \tag{22}$$

with R and S shown at the bottom of this page. The first two eigenvalues obviously have magnitude of unity. The other four eigenvalues have also magnitudes of unity. This is because $R \geq S$ and the square roots in the numerator of the expressions for $\lambda_3, \lambda_4, \lambda_5$, and λ_6 become real numbers. Therefore, we conclude that the proposed FDTD scheme is unconditionally stable regardless of the time step Δt. The Courant stability condition is then removed.

For reference, the eigenvalue expressions output directly by the MAPLEV5.2 we used is listed in Appendix. They are basically the long forms of (22).

IV. Numerical Results

To demonstrate the validity of the proposed FDTD method, an inhomogeneous rectangular cavity used in [5] was computed with both the proposed FDTD and the conventional FDTD. The geometry of the cavity is depicted in Fig. 1. One half of the cavity is filled with air and the other half with the dielectric material of a relative permittivity of $\varepsilon_r = 64$. The cavity has the dimension of 1 m $\times$ 2 m $\times$ 1.5 m. For both the proposed FDTD and the conventional FDTD, a uniform mesh with $\Delta l = 0.1$ m was used, leading to a mesh of $10 \times 20 \times 15$ grid points.

A. Numerical Verification of the Stability

Although we have theoretically proved that the proposed FDTD is unconditionally stable regardless of time step, numerical verification is necessary to confirm the theoretical result. Simulations were run for the inhomogeneous cavity with both the conventional FDTD and the proposed FDTD having a time step that exceeds the limit defined by the Courant condition (1), $\Delta t_{\mathrm{FDTDMAX}} = (\Delta l/c\sqrt{3}) = 1.92 \times 10^{-10}$ s in our case. Fig. 2 shows the electric field recorded at the center of the cavity. $\Delta t_{\mathrm{FDTD}} = 2 \times 10^{10}$ s was used with the conventional FDTD while a 100 times larger time step $\Delta t_i = 200 \times 10^{-10}$ ps was used with the proposed FDTD scheme. As can be seen, the conventional FDTD quickly becomes unstable [see Fig. 2(a)],

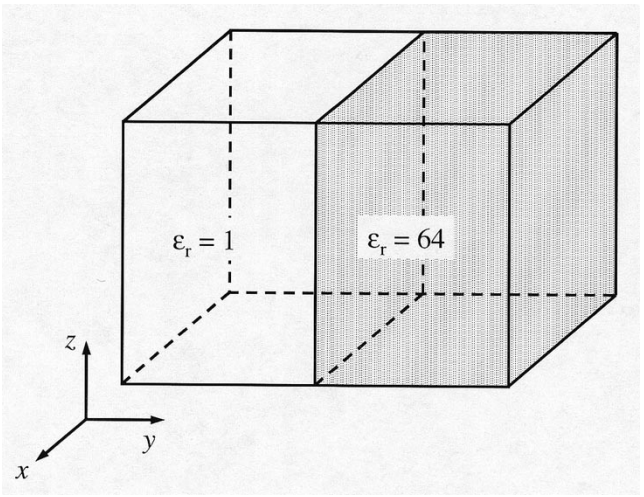

Fig. 1. Cavity half filled with air and the other half filled with dielectric material.

while the proposed FDTD remains with the stable solution [see Fig. 2(b)]. We also extended the simulation time to a much long period with the proposed scheme. No instability was observed.

B. Numerical Accuracy Versus Time Step

Since the proposed US-FDTD is now proved to be always stable, the selection of the time step is then no longer restricted by stability but by modeling accuracy. As a result, it is interesting and meaningful to investigate how the large time step will affect accuracy.

For the comparison purpose, both the conventional FDTD and proposed US-FDTD were used to simulate the cavity again. This time, the time step $\Delta t_{\mathrm{FDTD}} = 1.5 \times 10^{-10}$ s was chosen and fixed with the conventional FDTD, while the different values of time step Δt_i were used with the proposed FDTD to check for the accuracy. Table I presents the simulation results for the dominant mode in the cavity. As can be been, the relative errors of the proposed FDTD increase with the time step. These

$$\mathbf{\Lambda} = \begin{bmatrix} \frac{A_1+B_1}{Q_xQ_yQ_z} & \frac{2\mu\varepsilon W_xW_y}{Q_xQ_y} & \frac{2\mu\varepsilon W_xW_z}{Q_yQ_z} & \frac{-2j\mu W}{Q_xQ_y} & \frac{2j\mu^2\varepsilon W_z}{Q_yQ_z} & \frac{2j\mu D_1}{Q_xQ_yQ_z} \\ \frac{2\mu\varepsilon W_yW_x}{Q_zQ_x} & \frac{A_2+B_2}{Q_xQ_yQ_z} & \frac{2\mu\varepsilon W_yW_z}{Q_yQ_z} & \frac{2j\mu W}{Q_yQ_z} & \frac{2j\mu^2\varepsilon W_x}{Q_zQ_x} & \\ \frac{2\mu\varepsilon W_zW_x}{Q_zQ_x} & \frac{2\mu\varepsilon W_zW_y}{Q_xQ_y} & \frac{A_3+B_3}{Q_xQ_yQ_z} & \frac{2j\mu^2\varepsilon W_y}{Q_xQ_y} & \frac{2j\mu D_3}{Q_xQ_yQ_z} & \frac{-2j\mu W}{Q_zQ_x} \\ \frac{-2j\varepsilon W}{Q_xQ_z} & \frac{2j\varepsilon D_2}{Q_xQ_yQ_z} & \frac{2j\mu\varepsilon^2W_y}{Q_yQ_z} & \frac{A_1+B_3}{Q_xQ_yQ_z} & \frac{2\mu\varepsilon W_xW_y}{Q_yQ_z} & \frac{2\mu\varepsilon W_zW_x}{Q_zQ_x} \\ \frac{2j\mu\varepsilon^2W_z}{Q_zQ_x} & \frac{-2j\varepsilon W}{Q_yQ_x} & \frac{2j\varepsilon D_3}{Q_xQ_yQ_z} & \frac{2\mu\varepsilon W_xW_y}{Q_xQ_y} & \frac{A_2+B_1}{Q_xQ_yQ_z} & \frac{2\mu\varepsilon W_yW_z}{Q_zQ_x} \\ \frac{2j\varepsilon D_1}{Q_xQ_yQ_z} & \frac{2j\mu\varepsilon^2W_x}{Q_xQ_y} & \frac{-2j\varepsilon W}{Q_zQ_y} & \frac{2\mu\varepsilon W_zW_x}{Q_xQ_y} & \frac{2\mu\varepsilon W_yW_z}{Q_yQ_z} & \frac{A_3+B_2}{Q_xQ_yQ_z} \end{bmatrix} \tag{21}$$

$$R = \left(\mu\varepsilon + W_x^2\right)\left(\mu\varepsilon + W_y^2\right)\left(\mu\varepsilon + W_z^2\right)$$

$$S = \sqrt{4\mu\varepsilon\left(\mu\varepsilon W_x^2 + \mu\varepsilon W_y^2 + \mu\varepsilon W_z^2 + W_x^2W_y^2 + W_y^2W_z^2 + W_z^2W_x^2\right)\left(\mu^3\varepsilon^3W_x^2W_y^2W_z^2\right)}$$

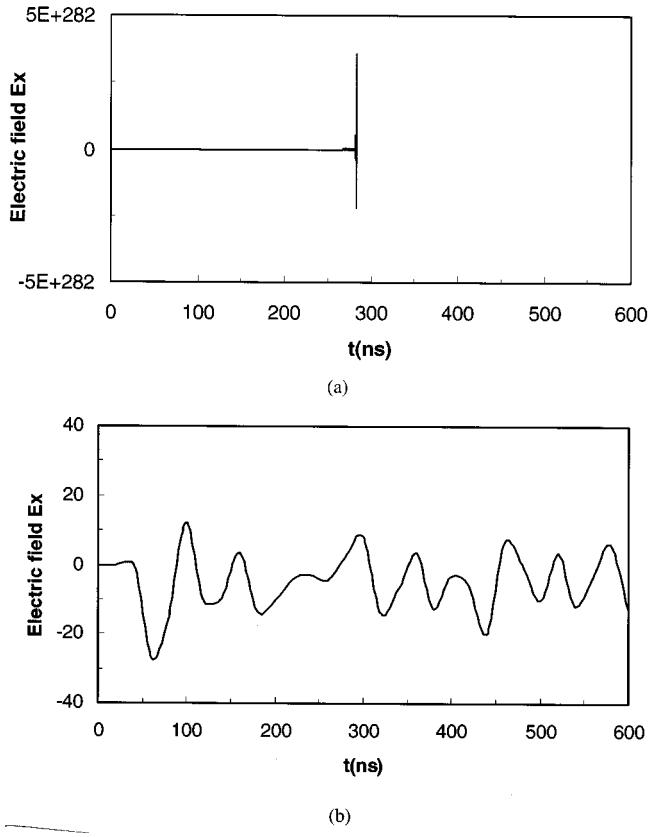

Fig. 2. Time-domain electric fields at the center of the cavity recorded with the conventional FDTD and the proposed US-FDTD. (a) Conventional FDTD solutions that become unstable with $\Delta t_j = 2 \times 10^{-10}$ s. (b) Proposed US-FDTD solution with $\Delta t_i = 200 \times 10^{-10}$ s.

TABLE I
PROPOSED US-FDTD SIMULATION RESULTS WITH DIFFERENT Δt

Analyt ical Result (MHz)	The proposed US-FDTD scheme					
	$\Delta t_{i1} = 4\Delta t_{FDTD}$		$\Delta t_{i2} = 6\Delta t_{FDTD}$		$\Delta t_{i3} = 8\Delta t_{FDTD}$	
	Result (MHz)	Relative error	Result (MHz)	Relative error	Result (MHz)	Relative error
18.627	18.587	0.21%	18.556	0.38%	18.511	0.62%

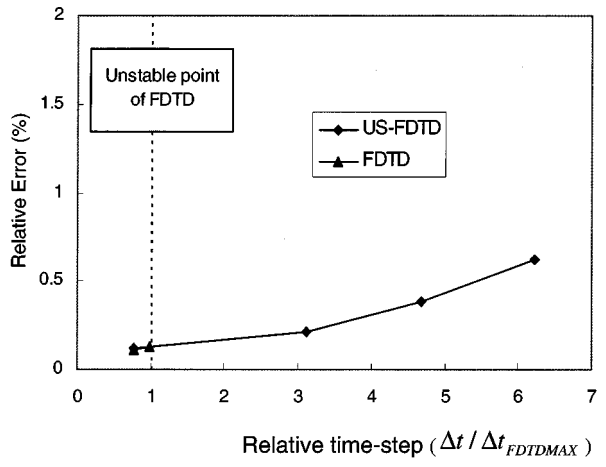

Fig. 3. Relative errors of the conventional FDTD and proposed FDTD as the function of relative time step $\Delta t/\Delta t_{\mathrm{FDTDMAX}}$. Dashed line represents the unstable point of the conventional FDTD scheme.

TABLE II
COMPARISONS OF RESULTS WITH CONVENTIONAL FDTD AND PROPOSED US-FDTD

Analytic Results (GHz)	Conventional FDTD scheme		Proposed US-FDTD scheme	
	Simulation results (GHz)	Relative error	Simulation results (GHz)	Relative error
18.627	18.587	0.21%	18.610	0.11%
27.172	27.046	0.46%	27.12	0.19%
29.374	29.155	0.88%	29.225	0.51%
32.881	32.626	0.77%	32.671	0.64%
35.069	34.832	0.67%	34.946	0.35%

errors are completely due to modeling accuracy of the numerical algorithm, such as the numerical dispersion. The tradeoff to the increased errors is, however, the reduction in the number of the iterations and therefore the shortening of the CPU time. In our experiments, for an error of 0.38%, the CPU time with the proposed FDTD is about half of that with the conventional FDTD, and for an error of 0.62%, the CPU time is cut to one third of the conventional FDTD time. Note that the increase in the time step or the reduction in the number of the iterations is not linearly proportional to the shortening of the CPU time. The reason is that the CPU time required for each time-step computation with the proposed FDTD is more than that with the conventional FDTD since the more components are involved in the computations [as seen from (10)].

Fig. 3 illustrates the relative errors for the dominant mode of the cavity computed using the conventional FDTD and the proposed FDTD with variable time steps. For clarity, relative time-step $\Delta t/\Delta t_{\mathrm{FDTDMAX}}$ is used. As can be seen, at low $\Delta t/\Delta t_{\mathrm{FDTDMAX}}$, the errors of both the conventional FDTD and the proposed FDTD are almost the same. However, after $\Delta t/\Delta t_{\mathrm{FDTDMAX}} = 1.0$, the conventional FDTD solutions diverge (become unstable) while the proposed FDTD continues to produce stable results with increasing errors that may or may not be acceptable depending on the applications and users' specifications.

C. Computational Expenditures

Since the Yee's grid is used with the proposed FDTD method, the number of field components at all the grid points is the same as that with the conventional FDTD. As a result, the memory requirement is in the same order as that for the conventional FDTD method.

On the other hand, as indicated in (10), more components are involved in the recursive computations at each time step with the proposed FDTD method. The CPU time for each time step with the proposed FDTD is then larger than that with the conventional FDTD method. However, since a larger time step can be used with the proposed FDTD, the total number of iterations required with the proposed FDTD could be reduced. The opposite effects of the more CPU time for each time step and the reduced number of iterations on the overall CPU time need to be studied, in particular, numerically. In the following paragraphs, a preliminary numerical experiment is presented.

Again, for the comparison purpose, both the proposed FDTD and the conventional FDTD were used to simulate the cavity. This time, the time step $\Delta t_{\mathrm{FDTD}} = 1.5 \times 10^{-10}$ s was chosen with the conventional FDTD, while $\Delta t_i = 4 \times \Delta t_{\mathrm{FDTD}} =$

6×10^{-10} s was chosen with the proposed US-FDTD. With such time step selections, we found, by trial and error, that the two methods presented similar accuracy. Therefore, the two methods can be compared in a fair manner. Twenty–thousand iterations were run with the conventional FDTD method, and 5000 iterations with the proposed FDTD. The iterations present the same physical time period since the time step with the proposed FDTD is four times of that with the conventional FDTD. Table II shows the first five resonant frequencies obtained with the two methods. The errors for the two methods are at the same level.

On a Pentium-III 450-MHz PC, it took 545.83 s to finish the simulation with the proposed FDTD and 873.34 s with the conventional FDTD. We then concluded preliminarily that a saving factor with the proposed FDTD in CPU time is about 1.6 when the conventional FDTD is used as a reference.

V. Discussions and Conclusions

In this paper, a new 3-D FDTD free of the Courant stability condition is presented for solving electromagnetic problems. In it, the Yee's grid is used but the alternative direction implicit technique is applied in formulating the algorithm. As a result, the memory requirement remains in the same order as that for the conventional FDTD while the time step is no longer restricted by the numerical stability but by the modeling accuracy of the FDTD algorithm. Analytical proof of the unconditional stability is shown and numerical verifications are presented to demonstrate the validity of the proposed method. Preliminary experiments indicated that with the same accuracy, the proposed method uses four times fewer iterations and is 1.6 times faster than the conventional FDTD.

The work of this paper, together with the earlier work reported by Nakimi and Ito [9], has presented a new direction in the continuing effort of the electromagnetic modeling community toward improving computational efficiency of the FDTD algorithms. It can be expected that because of the removal of the time step constraint in terms of the numerical stability, various efficient modeling techniques, such as multigridding scheme, can be implemented in an easier way. As to the future directions, since the time step is now solely determined by the accuracy of the model, naturally, the subsequent work is: 1) to investigate the errors of the proposed model (in particular the numerical dispersion properties) and 2) to develop an advanced model with higher accuracy. One of the possibilities of having an advanced model with smaller errors is to incorporate the MRTD principle into the proposed FDTD scheme. By doing so, it is expected that the time step can be increased to a much large value while the solution errors remain small because of the high accuracy of the MRTD model. In addition, since the MRTD allows the use of the number of the gird points much smaller than that for the conventional FDTD, the combined saving in time with the proposed method and in the grid size with the MRTD could be very significant. The investigation along this line is currently under way in our group.

In conclusions, the techniques such as MRTD opened a way for reduction in required computation memory while the proposed FDTD and the work in [9] presented a way in shortening the CPU time. Incorporation of both techniques could well result in an efficient FDTD algorithm that can handle electrically large electromagnetic structures effectively in the near future.

Appendix

The eigenvalues directly output by Maple V5.2.

$$
\begin{aligned}
\lambda_1 &= \lambda_2 = 1\\
\lambda_3 &= 1/2^*(-2^*Wy\hat{}2^*Wx\hat{}2^*\mu^*\varepsilon - 2^*Wz\hat{}2^*\mu^*\varepsilon^*Wx\hat{}2\\
&\quad + 2^*\mu\hat{}3^*\varepsilon\hat{}3 - 2^*\mu\hat{}2^*\varepsilon\hat{}2^*Wx\hat{}2\\
&\quad - 2^*Wz\hat{}2^*\mu\hat{}2^*\varepsilon\hat{}2\\
&\quad - 2^*Wy\hat{}2^*\mu^*\varepsilon^*Wz\hat{}2 + 2^*Wy\hat{}2^*Wx\hat{}2^*Wz\hat{}2\\
&\quad \times 2^*Wy\hat{}2^*\mu\hat{}2^*\varepsilon\hat{}2 + 4^*\\
&\quad \times \mathrm{sqrt}(-\mu\hat{}4^*\varepsilon\hat{}4^*Wy\hat{}2^*Wz\hat{}2\\
&\quad - \mu\hat{}5^*\varepsilon\hat{}5^*Wz\hat{}2 - \mu\hat{}2^*\varepsilon\hat{}2^*Wx\hat{}4^*Wy\hat{}2^*Wz\hat{}2\\
&\quad - \mu\hat{}5^*\varepsilon\hat{}5^*Wy\hat{}2 - \mu\hat{}5^*\varepsilon\hat{}5^*Wx\hat{}2\\
&\quad - \mu\hat{}2^*\varepsilon\hat{}2^*Wz\hat{}2^*Wy\hat{}4^*Wx\hat{}2\\
&\quad - \mu\hat{}2^*\varepsilon\hat{}2^*Wz\hat{}4^*Wx\hat{}2^*Wy\hat{}2\\
&\quad - \mu\hat{}4^*\varepsilon\hat{}4^*Wy\hat{}2^*Wx\hat{}2\\
&\quad - \mu\hat{}4^*\varepsilon\hat{}4^*Wx\hat{}2^*Wz\hat{}2 - \mu^*\varepsilon^*Wz\hat{}4^*Wx\hat{}4^*Wy\hat{}2\\
&\quad - \mu^*\varepsilon^*Wz\hat{}2^*Wy\hat{}4^*Wx\hat{}4\\
&\quad - \mu^*\varepsilon^*Wz\hat{}4^*Wy\hat{}4^*Wx\hat{}2))/(\mu\hat{}3^*\varepsilon\hat{}3\\
&\quad + Wz\hat{}2^*\mu^*\varepsilon^*Wx\hat{}2 + Wy\hat{}2^*\mu^*\varepsilon^*Wz\hat{}2 + Wy\hat{}2^*\\
&\quad \times Wx\hat{}2^*\mu^*\varepsilon + Wy\hat{}2^*\mu\hat{}2^*\varepsilon\hat{}2 + \mu\hat{}2^*\varepsilon\hat{}2^*Wx\hat{}2\\
&\quad + Wz\hat{}2^*\mu\hat{}2^*\varepsilon\hat{}2 + Wy\hat{}2^*Wx\hat{}2^*Wz\hat{}2)\\
\lambda_4 &= \lambda_3^*\\
\lambda_5 &= 1/2^*(-2^*Wy\hat{}2^*Wx\hat{}2^*\mu^*\varepsilon\\
&\quad - 2^*Wz\hat{}2^*\mu^*\varepsilon^*Wx\hat{}2 + 2^*\mu\hat{}3^*\varepsilon\hat{}3\\
&\quad - 2^*\mu\hat{}2^*\varepsilon\hat{}2^*Wx\hat{}2 - 2^*Wz\hat{}2^*\mu\hat{}2^*\varepsilon\hat{}2\\
&\quad - 2^*Wy\hat{}2^*\mu^*\varepsilon^*Wz\hat{}2 + 2^*Wy\hat{}2^*Wx\hat{}2^*Wz\hat{}2\\
&\quad - 2^*Wy\hat{}2^*\mu\hat{}2^*\varepsilon\hat{}2 + 4^*\\
&\quad \times \mathrm{sqrt}(-\mu\hat{}4^*\varepsilon\hat{}4^*Wy\hat{}2^*Wz\hat{}2\\
&\quad - \mu\hat{}5^*\varepsilon\hat{}5^*Wz\hat{}2 - \mu\hat{}2^*\varepsilon\hat{}2^*Wx\hat{}4^*Wy\hat{}2^*Wz\hat{}2\\
&\quad - \mu\hat{}5^*\varepsilon\hat{}5^*Wy\hat{}2 - \mu\hat{}5^*\varepsilon\hat{}5^*Wx\hat{}2\\
&\quad - \mu\hat{}2^*\varepsilon\hat{}2^*Wz\hat{}2^*Wy\hat{}4^*Wx\hat{}2\\
&\quad - \mu\hat{}2^*\varepsilon\hat{}2^*Wz\hat{}4^*Wx\hat{}2^*Wy\hat{}2\\
&\quad - \mu\hat{}4^*\varepsilon\hat{}4^*Wy\hat{}2^*Wx\hat{}2 - \mu\hat{}4^*\varepsilon\hat{}4^*Wx\hat{}2^*Wz\hat{}2\\
&\quad - \mu^*\varepsilon^*Wz\hat{}4^*Wx\hat{}4^*Wy\hat{}2\\
&\quad - \mu^*\varepsilon^*Wz\hat{}2^*Wy\hat{}4^*Wx\hat{}4\\
&\quad - \mu^*\varepsilon^*Wz\hat{}4^*Wy\hat{}4^*Wx\hat{}2))/(\mu\hat{}3^*\varepsilon\hat{}3\\
&\quad + Wz\hat{}2^*\mu^*\varepsilon^*Wx\hat{}2 + Wy\hat{}2^*\mu^*\varepsilon^*Wz\hat{}2 + Wy\hat{}2^*\\
&\quad \times Wx\hat{}2^*\mu^*\varepsilon + Wy\hat{}2^*\mu\hat{}2^*\varepsilon\hat{}2 + \mu\hat{}2^*\varepsilon\hat{}2^*Wx\hat{}2\\
&\quad + Wz\hat{}2^*\mu\hat{}2^*\varepsilon\hat{}2 + Wy\hat{}2^*Wx\hat{}2^*Wz\hat{}2)\\
\lambda_6 &= \lambda_5^*
\end{aligned}
$$

where

$$W_\alpha = \frac{\Delta t}{\Delta \alpha}\cdot \sin\left(\frac{k_\alpha \Delta\alpha}{2}\right), \qquad \alpha = x, y, z.$$

The first two eigenvalues are unity. Their magnitudes are one. For the other four eigenvalues, the arguments inside the square roots in the numerators are all negative numbers. As a result, the numerators are complex numbers. By taking the magnitudes of the numerators with MAPLE, we find symbolically that their values are exactly the same as the denominators. As a result, the magnitudes of the eigenvalues are unity.

ACKNOWLEDGMENT

The authors wish to thank the anonymous reviewers for their useful comments and constructive suggestions.

REFERENCES

[1] K. S. Yee, "Numerical solution of initial boundary value problems involving Maxwell's equations in isotropic media," *IEEE Trans. Antennas Propagat.*, vol. AP-14, pp. 302–307, May 1966.
[2] A. Taflove, *Computational Electrodynamics: The Finite-Difference Time-Domain Method*. Norwood, MA: Artech House, 1996.
[3] P. H. Aoyagi, J. F. Lee, and R. Mittra, "A hybrid Yee algorithm/scalar-wave equation approach," *IEEE Trans. Microwave Theory Tech.*, vol. 41, pp. 1593–1600, Sept. 1993.
[4] M. Mrozowski, "A hybrid PEE-FDTD algorithm for accelerated time domain analysis of electromagnetic wave in shielded structrues," *IEEE Microwave Guided Wave Lett.*, vol. 4, pp. 323–325, Oct. 1994.
[5] M. Krumpholz and L. P. B. Katehi, "MRTD: New time-domain schemes based on multiresolution analysis," *IEEE Trans. Microwave Theory Tech.*, vol. 44, pp. 555–571, Apr. 1996.
[6] Q. H. Liu, "The pseudospectral time-domain (PSTD) method: A new algorithm for solution of Maxwell's equations," in *Proc. IEEE Antennas and Propagation Society Int. Symp.*, vol. 1, 1997, pp. 122–125.
[7] R. Holland, "Implicit three-dimensional finite differencing of Maxwell's equations," *IEEE Trans. Nucl. Sci.*, vol. NS-31, pp. 1322–1326, 1984.
[8] P. M. Goorjian, "Finite difference time domain algorithm development for Maxwell equations for computational electromagnetism," in *Proc. IEEE Antennas and Propagation Society Int. Symp.*, vol. 1, 1990, pp. 878–881.
[9] T. Namiki and K. Ito, "A new FDTD algorithm free from the CFL condition restraint for a 2D-TE wave," in *IEEE Antennas Propagat. Symp. Dig.* , July 1999, pp. 192–195.
[10] G. D. Smith, *Numerical Solution of Partial Differential Equations*, Oxford, U.K.: Oxford Univ. Press, 1978.
[11] D. W. Peaceman and H. H. Rachford, "The numerical solution of parabolic and elliptic differential equations," *J. Soc. Ind. Appl. Math.*, vol. 42, no. 3, pp. 28–41, 1955.

Fenghua Zheng (S'99) received the B.Eng. degree from the University of Science and Technology of China, Hefei, China, in 1994, and the M.A.Sc. degree from Shanghai Institute of Technical Physics, Shanghai, China, in 1997. He is currently working toward the Ph.D. degree at Dalhousie University, Halifax, NS, Canada.

His research interests include numerical techniques for modeling electromagnetic fields, computer-aided design of microwave and millimeter-wave circuits, and wireless propagation channel modeling.

Zhizhang Chen (S'92–M'92–SM'96) received the B.Eng. degree from Fuzhou University, Fuzhou, China, in 1982, and the Ph.D. degree from the University of Ottawa, Ottawa, ON, Canada, in 1992.

From January of 1993 to August of 1993, he was an Natural Science and Engineering Research Council (NSERC) Postdoctoral Fellow with the Department of Electrical and Computer Engineering, McGill University, Montreal, PQ, Canada. In 1993, he joined the Department of Electrical and Computer Engineering, DalTech, Dalhousie University, Halifax, NS, Canada, where he is presently an Associate Professor. Currently, he is a Visiting Faculty Member with the Department of Electrical and Electronic Engineering, The Hong Kong University of Science and Technology, Kowloon, Hong Kong. His research interests include RF/microwave electronics, numerical modeling and simulation, and antenna designs for wireless and satellite communications.

Jiazong Zhang received the M.Sc. (with honors) and Ph.D. degrees in 1995 and 1998, respectively, from the Department of Radio Engineering, Southeast University, China.

He is currently a Postdoctoral Fellow with DalTech, Dalhousie University, Canada. His research interest includes computational electromagnetics, passive antenna, active integrated antenna, and RF/microwave circuits and devices analysis and design.